Bulletin of the Seismological Society of America, Vol. 84, No. 5, pp. 1310–1326, October 1994

Seismic Waveform Modeling in the Los Angeles Basin

by Craig W. Scrivner and Donald V. Helmberger

Abstract The proximity of several recent earthquakes to the Los Angeles sedimentary basin provides an opportunity to isolate the effects of the basin on wave propagation. The 4 October 1987 aftershock (M_L = 5.3) of the Whittier Narrows sequence and the 28 June 1991 Sierra Madre mainshock (M_L = 5.8) are on a similar azimuth to stations overlying the deepest part of the basin. A distinctive feature of records from basin stations recording the 4 October aftershock is the large amplitude of multiple *S*, *SS*, *etc*. The multiples have up to twice the amplitude of the direct *S* phase on the tangential component. At such a short range, less than 25 km, a horizontal seismic velocity gradient is needed to turn rays rapidly enough for large-amplitude multiples to form. A forward modeling approach is employed, using finite-difference numerical techniques that produce double-couple point-source solutions. A model based on a recent geologic cross section constructed for the east edge of the Los Angeles Basin generates more phases than are seen in the seismic records. Simpler models, based on dipping layers with low shear velocities in the top few layers, fit the data better. The seismic velocity, depth, and dip of the layers are varied to fit the timing between the direct *P*, the direct *S*, and the first *S* multiple. The timing and amplitude of the direct and first multiple *S* pulses are well modeled, though the phase of the first multiple does not match the data. Including a steeply dipping west edge in the basin model has little effect on the synthetic waveforms, except at distances near that basin edge. The amplitude of *SS* is greatest in the deepest part of the basin, where it is two times larger than direct *S*. The coda duration increases from 8 sec to more than 20 sec from the NE to the SW. The Sierra Madre mainshock occurred about 25 km to the NE of the Whittier Narrows sequence. The model for Whittier Narrows was extended to this distance, with a shallow basin between Whittier and the Sierra Madre hypocenter to simulate the San Gabriel sedimentary basin. Phases generated by the edge of the deep basin continue to dominate the synthetic waveforms, but this model generates a lengthy coda. This study shows that specific phases with frequencies up to 1 Hz that have traveled through deep sedimentary basins can be explained by two-dimensional seismic velocity models.

Introduction

Events such as the 1985 Michoacan earthquake have dramatically demonstrated that it is important in seismic hazard analysis to understand the effects of sedimentary basins on the propagation of seismic energy (Anderson *et al.*, 1986; Campillo *et al.*, 1989; Kawase and Aki, 1989). There are a number of other areas in the world, including Los Angeles, where large populations live on or near sedimentary basins. Parts of the Los Angeles sediment-filled basins extend as deeply as 9 km (Yerkes *et al.*, 1965; Davis *et al.*, 1989). The geometry of the Los Angeles basin is shown in Figure 1. There is long-standing concern about the effect of this basin on the amplitude and duration of shaking that will be felt in the Los Angeles area as the result of a large earthquake on the San Andreas Fault. In addition, there is concern about damaging events in the Los Angeles area itself. This concern was originally produced by the 1933 Long Beach earthquake on the Newport–Inglewood fault zone, and has been raised again by recent quakes on blind thrusts adjacent to the basin (Hauksson, 1990).

Waveforms recorded in sedimentary basins are affected by the three-dimensional structure of the basin. The effect is minimized for recordings of teleseismic events; body waves arrive with near-vertical incidence

through the bottom of the basin, and long-period surface waves average out basin effects with the surrounding structure. Even so, "site response" has a significant effect on these waveforms. Near-field events interact strongly with the basin edge (the interface between basement rocks and compacted sediments). This interface can be curved tightly enough to introduce three-dimensional multipathing effects. In addition, the bottom of the basin is likely to be irregular and the stratigraphic units, which may roughly correlate with the seismic velocity structure, may be folded or tilted. Synthetic waveforms based on three-dimensional velocity models of sedimentary basins have been generated (Frankel and Vidale, 1992; Graves and Clayton, 1992), and these results confirm the effectiveness of the basins for trapping seismic energy, increasing peak amplitudes, and extending the waveform coda. Comparisons between synthetic waveforms and data in these studies, however, are based on the similarity of the general shape of the envelope of the waveforms, on patterns of peak accelerations for the distribution of stations, or on the similarity of parameters derived from the synthetic waveforms to empirical relationships. At-

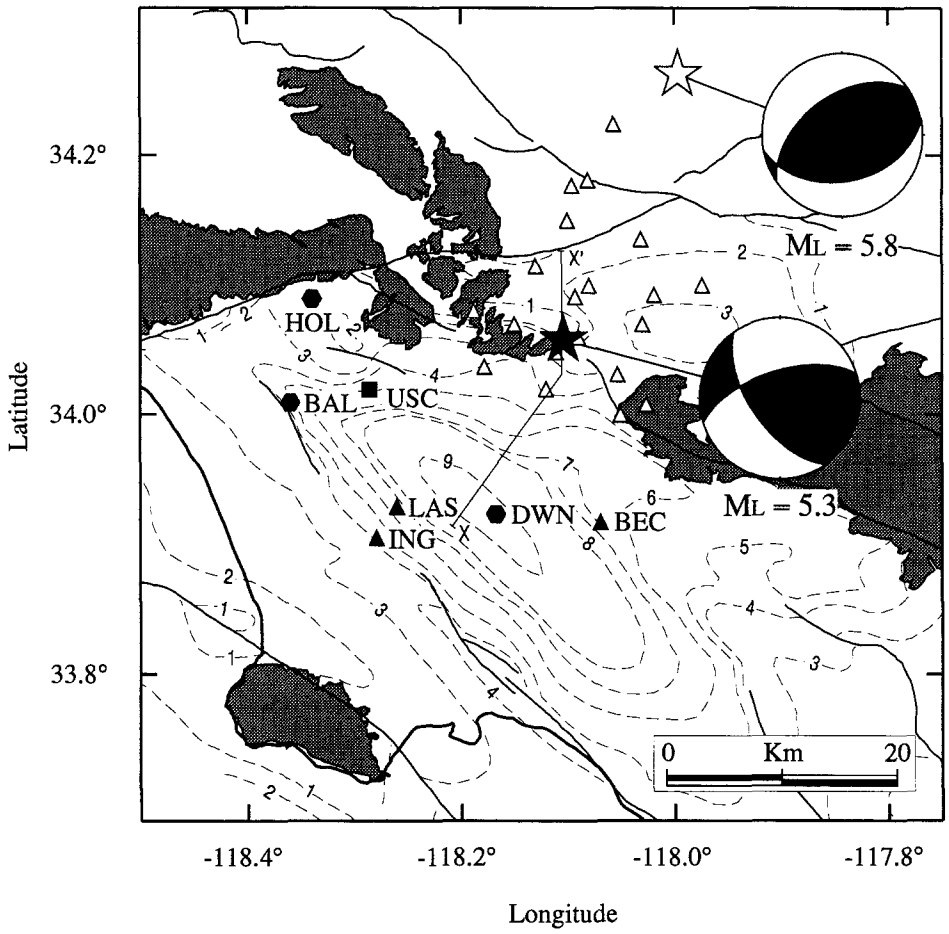

Figure 1. Map indicating the epicenters and focal mechanisms of the 4 October 1987 Whittier Narrows aftershock and the 28 June 1991 Sierra Madre mainshock with the surrounding seismic stations. The Whittier Narrows aftershock is the black star and the Sierra Madre mainshock is the white star. The shaded portions of the focal mechanisms are compressional. Triangles, squares, and hexagons indicate seismic station locations. The black symbols are for stations that are used in this study. Hexagons indicate records that are available for both events (stations DWN, BAL, and HOL). The black triangles indicate stations BEC, LAS, and ING, for which only Whittier Narrows aftershock records were used in this study. Only a record for Sierra Madre was available from station USC (the square). The stippled regions of the map are the hills surrounding the Los Angeles basin. The solid lines indicate a few of the significant faults in the region. The dashed contours indicate the depth in kilometers (below sea level) to crystalline rock in the Los Angeles sedimentary basin (from Yerkes *et al.*, 1965). The line X-X′ through the Whittier Narrows area is the location of the cross section in Davis *et al.* (1989) on which the model in Figure 5 is based.

tempts to model specific phases in data have not been made with three-dimensional structures because the number of parameters to vary in the velocity models is immense and the cost of generating synthetic waveforms is prohibitive.

Even with one-dimensional models, it is possible to successfully forward model some phases in seismic data from receivers in sedimentary basins. Modeling the polarity and amplitude of the direct arrivals is an example. Figure 2 shows the fit of velocity data and synthetic waveforms for the direct *S* arrival from the large 4 October 1987 aftershock of the Whittier Narrows sequence on tangential component records at strong-motion stations in the San Gabriel and Los Angeles basins. The reversal of polarity of the direct arrival across radiation pattern nodes is clear in the data set. However, the amplitudes of the phases at nodal stations do not fall off to values as low as is theoretically expected. Examples of this are SAG and ELM in the San Gabriel basin. This suggests that multipathing effects of the basin average out amplitude variations at the nodes. The one-dimensional model only predicts the direct phase well. It does not produce multiples like those seen in the data at stations LAS, ING, and BEC in Figure 2.

Since a one-dimensional velocity model can fit the direct *S* arrival, it is reasonable to expect that some other phases can be fit by the two-dimensional structure along the azimuth between the epicenter and the receiver. One way to assess the appropriateness of a two-dimensional velocity structure is simply to see how cleanly the horizontal components of the seismogram rotate into the radial-tangential orientation. If seismic energy is arriving off-azimuth, then the tangential component will have significant *P*-wave amplitudes. However, polarization analysis, such as that suggested by Vidale (1986), provides a clearer picture of the directions from which energy is reaching the receiver when an arrival is separated in time from other arrivals. Vidale's method gives quan-

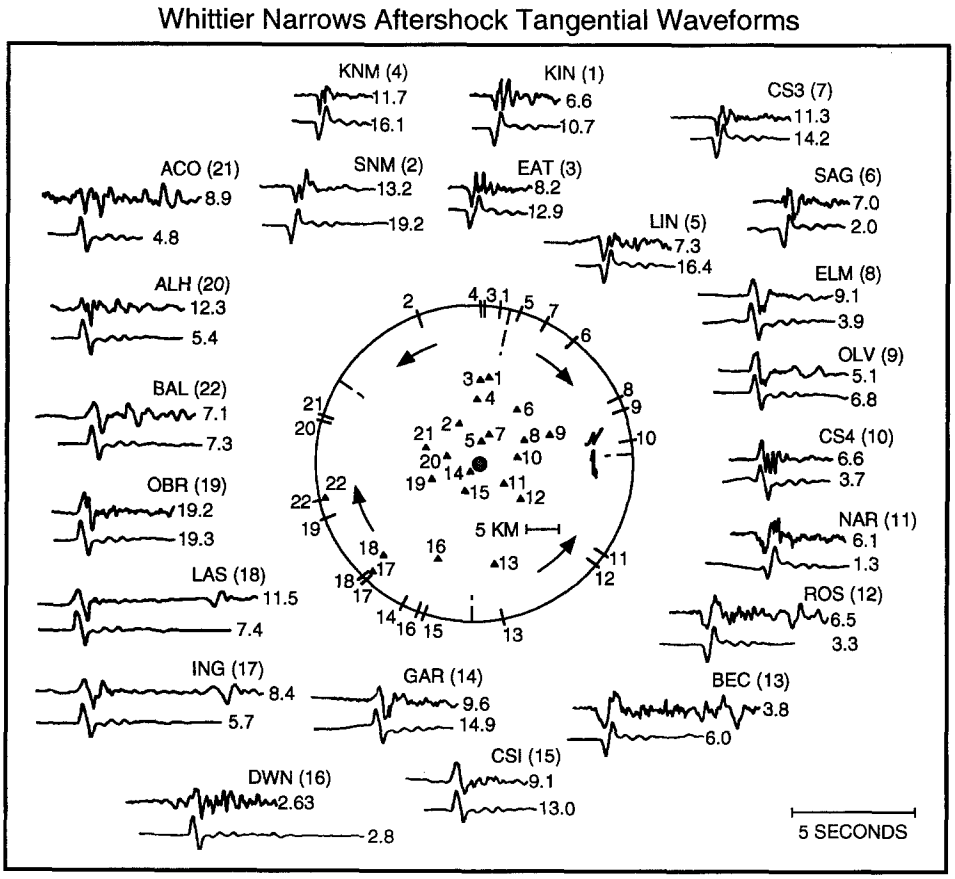

Figure 2. Comparison of velocity data and synthetic waveforms generated with a flat-layer model. The relative station locations are plotted in the circle, and the aftershock epicenter is located at the center of the circle. Dashed lines are approximate nodal planes as indicated by the first-motion polarity of the data. While the polarity changes are clear, the peak amplitudes of the data from stations near the nodal planes do not drop to the low values predicted by the synthetic waveforms. The synthetics were made using the one-dimensional model of Saikia (1994).

titative values of the strike (relative to the backazimuth) and dip of the plane of maximum polarization of incoming waves, rather than the more qualitative indications of waveform polarization found in particle motion plots.

A two-dimensional model is only directly applicable to a particular cross section. If data from multiple stations, situated over a range of azimuths from the source, are to be modeled, then the model will correspond to an average structure across the azimuth range. Also, a two-dimensional model cannot reproduce three-dimensional multipathing effects on the propagation of seismic energy. In counterbalance to these limitations of two-dimensional models, the computation of synthetic waveforms in two dimensions is faster and cheaper than in three dimensions. More iterations can be made to develop a model. A three-dimensional model produces an overall picture of how seismic energy propagates through an area. However, such a model is based on sources of information, such as seismic reflection lines, well data, and geological structural models, that are of limited density and resolution. This may result in a model that overlooks a significant aspect of the seismic energy propagation through the structure. Thus, two-dimensional modeling can be used to fine-tune cross sections through three-dimensional models and help constrain the models as a whole.

Method

The two earthquakes discussed in this article are the 4 October 1987 Whittier Narrows aftershock (M_L = 5.3) and the 28 June 1991 Sierra Madre mainshock (M_L = 5.8). A location map is shown in Figure 1. The 4 October event was the largest aftershock in the Whittier Narrows sequence, but it was a much simpler event than the 1 October mainshock. The aftershock was predominately strike slip; the mainshock was almost pure thrust. The entire sequence took place directly adjacent to the Los Angeles basin and was associated with the Elysian Park Thrust (Hauksson, 1990). This sequence was a clear indication that such blind thrusts need to be considered in seismic hazard assessments for the area. The 28 June 1991 Sierra Madre mainshock was 25 km further away from the edge of the Los Angeles basin than the Whittier Narrows sequence, and the shallow San Gabriel basin lies in between. It was, however, at about the same azimuth from stations in the Los Angeles basin as the Whittier Narrows sequence. This allows us to extend the model further back from the basin, and look at how the effect of the basin on waveforms changes as the source is moved away from the basin's edge.

We first work with data from six stations in the Los Angeles basin area for the Whittier Narrows aftershock (Fig. 3). All three components of data are available from each of these stations. The stations LAS, ING, DWN, HOL, and BAL are California Strong Motion Instrumentation Program, Division of Mines and Geology (CDMG) instruments (Shakal *et al.*, 1987). The sensors record acceleration with free periods of about 0.0395 sec and damping coefficients of around 0.59. The response is flat in acceleration to about 10 Hz. The raw acceleration has been resampled to a rate of 50 samples per second and bandpass-filtered with ramps of about 0.3 to 0.6 Hz and 23.0 to 25.0 Hz during CDMG processing. The BEC station is a GEOS instrument installed and maintained by the U.S. Geological Survey (USGS). The nominal parameters for this instrument are a free period of 0.02 sec and a damping coefficient of 0.7 (Mueller *et al.*, 1988). This results in a response that is flat to acceleration out to about 20 Hz. The BEC station is at an azimuth to the southeast of the others, where the basin is about 7 km deep. Both the BEC and DWN stations are at a 16-km distance from the epicenter of the 4 October aftershock. Stations HOL and BAL are on the north rim of the basin where sediments are relatively thin. The ING and LAS stations are near the Newport–Inglewood fault zone at the west edge of the Los Angeles basin. Only station DWN lies over the deepest Los Angeles basin.

The records from these stations, except for HOL and BAL, contain a very strong phase on the tangential and radial components 5 to 6 sec after the direct *S* arrival. Complex polarization analysis (Vidale, 1986), an example of which is given in Figure 4, shows that on the records from DWN, BEC, ING, and LAS the dip of the polarization plane of this phase is close to 0° and the strike is more than 60° away from the backazimuth. This is consistent with a shear wave arriving on azimuth from the source, without heavy contamination by energy refracted from other parts of the basin. On the DWN tangential velocity record, this phase is more than two times larger than direct *S* pulse. We argue that this phase is appropriately modeled as a first multiple (*SS*) off the bottom of the basin of the direct *S* ray, that its appearance in the records is dependent on the seismic structure of the edge of the sedimentary basin, and that it therefore can be approximately modeled with a two-dimensional velocity structure.

To work with two-dimensional velocity models, we have generated the synthetic waveforms by a finite-difference formulation described in Vidale *et al.* (1985). In this approach, the *SH* and *P-SV* systems are decoupled and solved separately. It is based on using known first-term asymptotic solutions for double-couple sources to introduce pseudo-near-field terms, which produce the appropriate radiation patterns for a point source with two-dimensional codes. These asymptotic approximations break down for long periods because of the neglect of near-field terms. Also, the grid used in the finite-difference modeling introduces high-frequency dispersion, with the severity of this effect controlled by the size of the grid elements. As a result, the synthetic waveforms pro-

duced are inherently bandlimited. In this study, the synthetics have been bandpass-filtered to minimize the long-period and high-frequency artifacts. The calculations are appropriate for a line source perpendicular to the two-dimensional cross section and point-source solutions are generated from these by a simple transformation (Helmberger and Vidale, 1988).

One approach to modeling the data is to use a geologic cross section as a starting point. We have constructed a model directly from the cross section developed by Davis *et al.* (1989) that passes through the Whittier Narrows area (Fig. 5). The position of this cross section is shown as the line X-X′ on the map in Figure 1. Calculations for this model with the two-dimensional finite difference code with a double-couple source at the depth and location relative to the edge of the basin that are appropriate for 4 October event result in synthetic waveforms that are much more complex than the data. It is apparent that this model needs to be smoothed to fit the data. We start from a simple one-dimensional seismic velocity model and tried to construct a simple two-dimensional model that satisfies the data. We use a deterministic forward modeling approach to satisfy the clear signals in the data.

The effect of the basin edge is to weaken the direct phase and to enhance the reflected phases (Fig. 6). The ray for the direct phase intersects the bottom of the basin obliquely where the interface is flat. As a result, the transmission coefficient for this ray into the basin is very small. In comparison, the ray for the reflected phases is nearly normally incident on the dipping edge of the basin. This ray has a transmission coefficient closer to 1 than does the direct ray. In addition, the lateral velocity gradient at the edge of the basin turns the ray of the multiple shallowly within the basin edge at greater than critical angle. Therefore, all of the transmitted energy

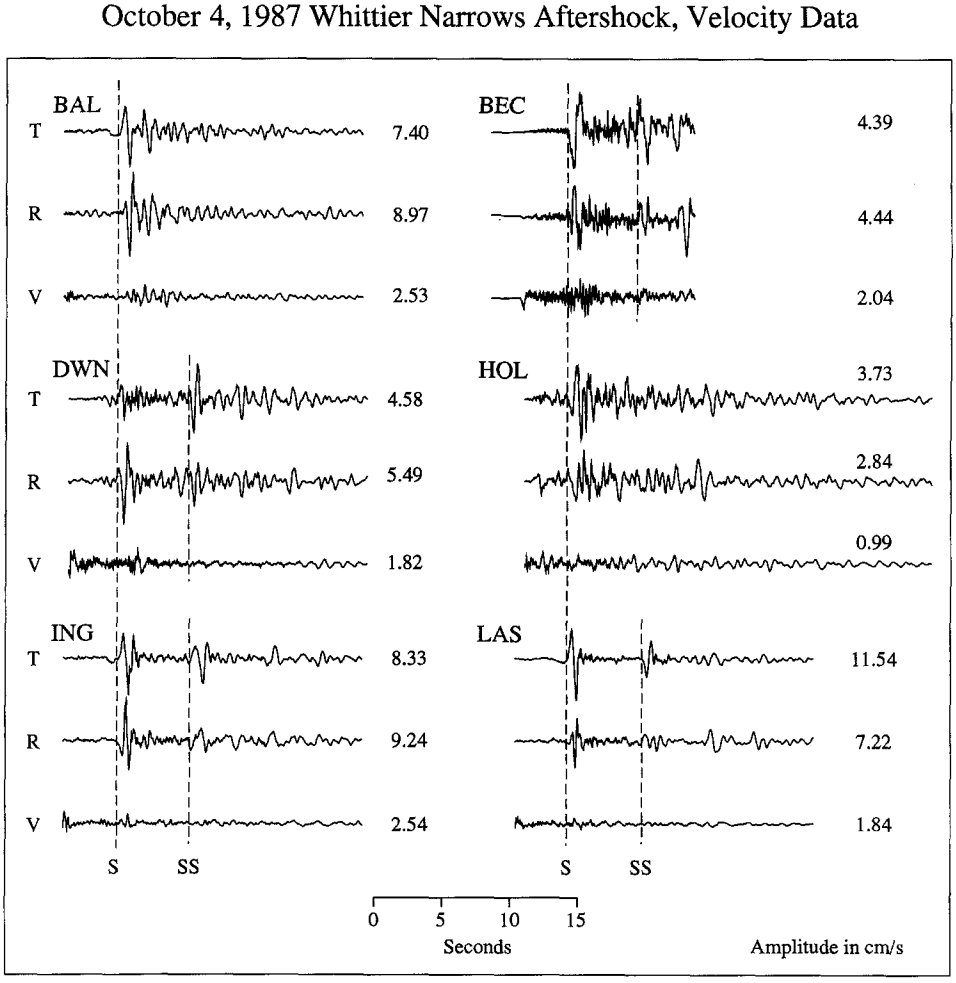

Figure 3. Three-component velocity records from six stations in the Los Angeles basin for the 4 October 1987 Whittier Narrows aftershock. The strong shear-wave multiple is evident in the tangential components at the stations near the central basin. DWN, ING, LAS, BAL, and HOL are instruments maintained by the California Division of Mines and Geology (CDMG). BEC is a USGS GEOS station. Amplitudes are in centimeters per second.

gets trapped by the shallow structure and is channelled into the multiple *S* phases.

Results

Our preferred model fits the relative amplitude of the *SS* and *S* phases, *S-P* times for the data, and absolute *S* and *P* times (for those stations where they are available). The fit is best for the stations over the deep basin (DWN, BEC, and LAS). The modeling was done primarily for the *SH* system because *P-SV* waveforms are more expensive to synthesize and more complicated to treat because of conversions between *P* and *S* energy at interfaces. For the best-fit model, however, we also calculated radial and vertical synthetic waveforms.

The finite-difference code calculates synthetic waveforms for the fundamental fault orientations. For the *SH* system, this is vertical strike-slip and vertical dip-slip (Fig. 7). In the corresponding synthetics, the multiple is clearly present for both fault types. However, the strike-slip fault orientation produces a lower-amplitude multiple than is needed. The dip-slip synthetics have very strong multiples, and this suggests that the strength of this multiple in records such as DWN is due to the small dip-slip component of the aftershock source mechanism. Synthetic waveforms are compared with the velocity data in Figure 8a.

An emphasis was placed on fitting the records from station DWN (see Fig. 8b) because DWN is the only station in the data set over the deepest part of the Los Angeles basin and the multiple on the tangential component is particularly strong for this station. Unfortunately, the trigger time was not recorded by the DWN station, so the data and synthetic waveforms are lined up by the direct *S* arrival on the tangential component. The dashed line indicates this point for all the waveforms. The amplitude scale for the synthetic waveforms is about twice

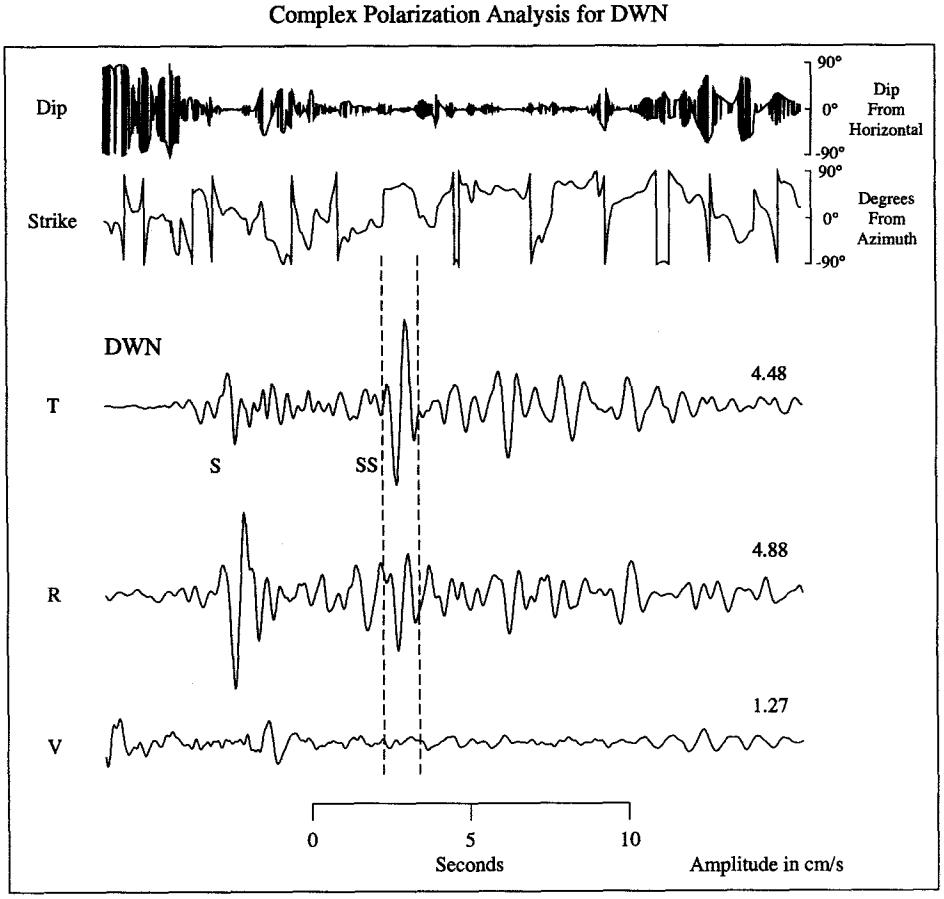

Figure 4. An example of complex polarization analysis (Vidale, 1986). The analysis is for station DWN. The velocity data was lowpass-filtered with a corner at 4-Hz frequency prior to the analysis, in order to smooth the results. The dip and strike relative to the backazimuth of the polarization plane are shown as a function of time and range from −90° to 90°. A portion of the record around the multiple phase that is being modeled is shown by dashed lines. The large and rapidly fluctuating values for the dip at the beginning of the time series are artifacts of the low amplitude of the horizontal components prior to direct *S*.

that of the data when a moment of 5×10^{23} dyne-cm is used to construct the synthetics. The tangential component has the best fit of synthetic to data among the three components. The relative timing and amplitude of the *SS* and *S* arrivals in the data are well matched in the synthetic. There is also a suggestion of an additional multiple 4 sec after *SS* in both the data and the synthetic, which would correspond to *SSS*. The radial component of the data has more phases than are found in the synthetic. One reason for this may be that *P* to *S* conversions at the edge of the basin are not strongly generated by this model. The *P*-wave velocities in the model are only crudely established, and the homogeneity of the *P* velocity in the top of the model is certainly not accurate. The *SS* phase in the data is larger than the multiple in the synthetic, and the additional multiple (at 12 to 13 sec) is present in the data but not the synthetic. This suggests that *SH* energy is being turned onto the radial component by the three-dimensional structure of the basin, but not so strongly that it obscures the two-dimensional propagation of most of the energy. The vertical component is much lower amplitude in both the data and the synthetic. It is interesting to note that the direct *S* phase is not visible on the vertical component of the data. This indicates that the direct shear wave is arriving with vertical incidence. The dashed line in Figure 8b indicates where direct *S* arrives on the radial and tangential components. The phase coming in 5 to 6 sec after the trigger on the vertical component is probably a converted *S* to *P* multiple phase. The vertical synthetics have both the direct and the converted phase. This suggests that the shallow shear-wave velocities in our model are

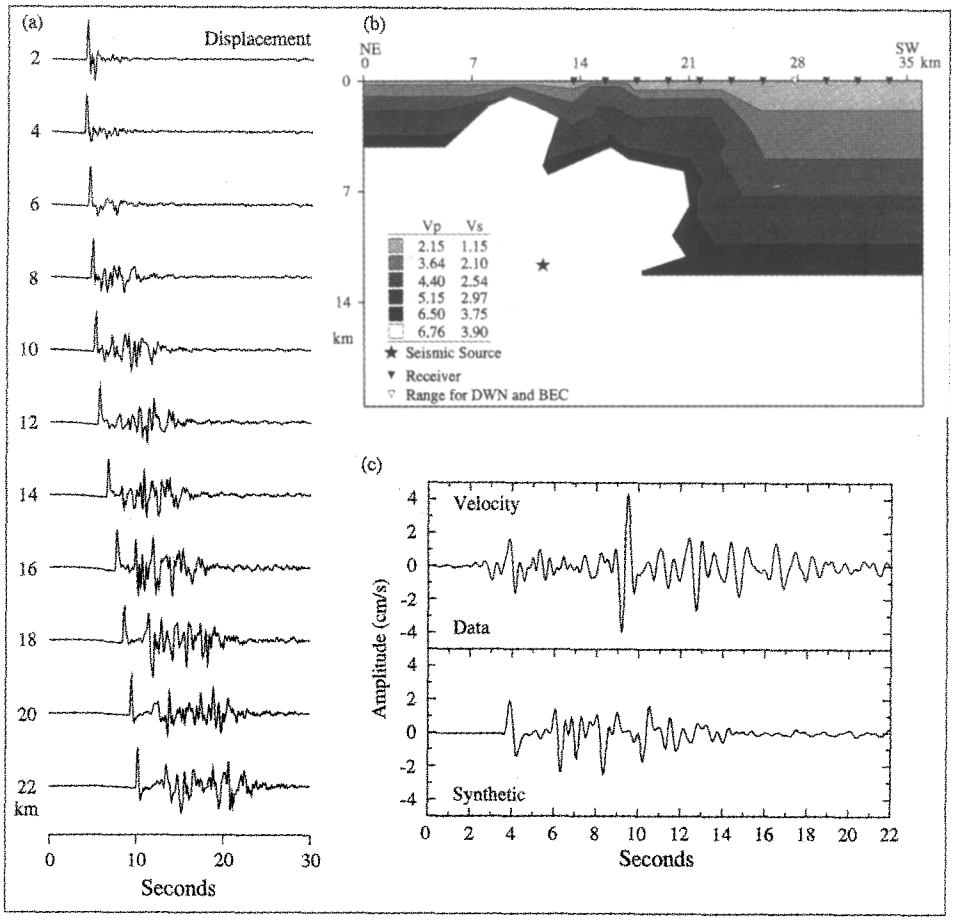

Figure 5. (a) Finite-difference synthetic waveforms of the tangential-displacement component for the 4 October 1987 Whittier Narrows aftershock along the DWN azimuth for distances from 2 to 22 km. The source mechanism used to construct these synthetics is from Saikia (1994). (b) The seismic velocity model used to calculate the synthetic waveforms in part (a). The velocity structure is an attempt to directly incorporate the geologic cross section of Davis *et al.*, 1989. Velocities are given in kilometers per second. NE is to the left. (c) A comparison of the tangential component velocity data from station DWN with the velocity synthetic at the correct range from the source (16 km). The two waveforms are lined up on the direct *S* phase. A source with $M_0 = 5 \times 10^{23}$ dyn-cm was included in the synthetic waveforms.

not slow enough to turn the direct *S* ray to vertical incidence.

Trigger times are known for three of the six available stations, ING, LAS, and BAL. The data and synthetic waveforms for these stations are compared in absolute time in Figure 8a. The trigger times for stations BEC, DWN, and HOL are not known. The data and synthetics for these stations are lined up on the direct *S* of the tangential component. As mentioned before, the modeling in this study was primarily done on the tangential component, to avoid the cost and added complexities of fitting the *P-SV* system. In addition, the model cannot hope to fit all the data on azimuths from 169° to 279°, the contours of basin depth in Figure 1 indicate the differences in the cross sections from the hypocenter to each station. The stations DWN, ING, and LAS are on azimuths for which the propagation path should be similar. The absolute timing of the direct *S* for ING and LAS are within a second of the data. The relative timing of the *SS* and the direct *S* arrivals for stations DWN and LAS are quite good. However, the synthetic for ING does not predict a strong *SS* arrival, though the data for this station has a clear signal. The absolute amplitude of the whole waveforms and the relative amplitudes of the *SS* and *S* arrivals on the synthetics are fit within a factor of 2. The relative phase of the *SS* arrival to that of the direct *S* is not well predicted by the synthetic waveforms. The synthetic *SS* is consistently shifted 90° in phase relative to the direct *S*, as expected. The data for stations DWN and LAS suggest that the multiple is 180° out of phase with the direct *S* arrival. The *SS* arrival in the data at station ING, however, seems not to be phase-shifted at all relative to the direct *S*. Stations BEC, BAL, and HOL are on azimuths from the hypocenter that do not cross the deepest portion of the basin. Of the three, BEC is over the deepest sedimentary layer, and there is a large-amplitude multiple on the data for this station, but not for the other two. However, the synthetic waveforms for these azimuths do not predict large multiples, so it is unclear whether such multiples are missing from the data because of the shallow basin structure or because of the radiation pattern.

The modeling was primarily concerned with matching the tangential component and so it is not surprising that the vertical and radial synthetic waveforms, generated by the *P-SV* calculation, do not fit the data as well as the tangential component. The timing is still fairly good between different phases, but the absolute amplitudes are less consistent. Also, the relative amplitudes of the phases are not as consistent for the vertical and radial synthetic waveforms.

The model just discussed included only the east edge of the Los Angeles basin. It might be argued that energy propagating across the basin would be reflected back at its west edge and be trapped (Novaro *et al.*, 1990). This would produce a ringing effect that would complicate and lengthen the waveform. When such an edge is included in the model, however, there are almost no changes seen in the synthetic waveforms (Fig. 9). In the middle of the basin, there is no effect at all on the strong multiple to the direct *S* phase. Stronger effects can be seen at the west basin edge, but they are still minor. The west basin edge probably produces more significant effects beyond the basin by disrupting surface waves across the basin and by setting up a further set of focused phases in offshore sedimentary basins. Such effects would be consistent with the results of Vidale and Helmberger (1988).

The Whittier Narrows sequence was unusual because it occurred so close to the edge of the Los Angeles basin. Although concern is increasing about the threat posed by basin-bounding faults, it is also important to see whether the focusing effects modeled above persist for a seismic source farther from the basin. Since the 28 June 1991 Sierra Madre earthquake is along a similar azimuth to the basin as the Whittier Narrows aftershock, it is a useful event to consider. Unfortunately, records from strong-motion stations in the Los Angeles basin for the Sierra Madre mainshock are not numerous. There are CDMG records from the DWN, BAL, and HOL stations and a record from a Guralp instrument at USC (Fig. 10). Synthetic waveforms were calculated using the source location and parameters of Dreger and Helmberger (1991), except that a lower moment was used than was found in that study. Wald (1992) and Helmberger *et al.* (1993) argue that most of the high-frequency energy produced by this event was generated in the area near the hypocenter where there was high stress drop and about 30% of the moment was produced.

Displacement synthetics for the azimuth to the station DWN with the Sierra Madre mainshock source

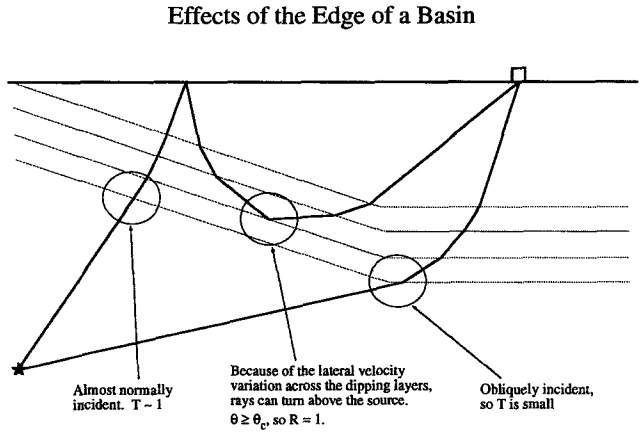

Figure 6. A cartoon indicating the effect, in terms of ray theory, of the edge of a sedimentary basin on propagating seismic energy. The solid star at the left is the seismic source, and the box at upper right is the receiver. The dashed lines are interfaces between velocity layers.

mechanism are shown in Figure 11 for two models. The first model shown is simply the Whittier Narrows model extended as a flat-layer model, back far enough to cover the Sierra Madre source. For receivers over the deep basin, the time for the arrival of the direct S and following phases is obviously longer, but the waveform following the direct S is the same as that of the Whittier Narrows model. We have also included a basin edge near the Sierra Madre source in an attempt to model the effect of the San Gabriel basin on wave propagation into the Los Angeles basin. The direct S and multiples are still unaffected by this additional complexity, but there is a much longer wave train at ranges out into the Los Angeles basin. This model does not include the ridge that exists (at least for some azimuths) between the San Gabriel and Los Angeles basins. This would be expected to shorten

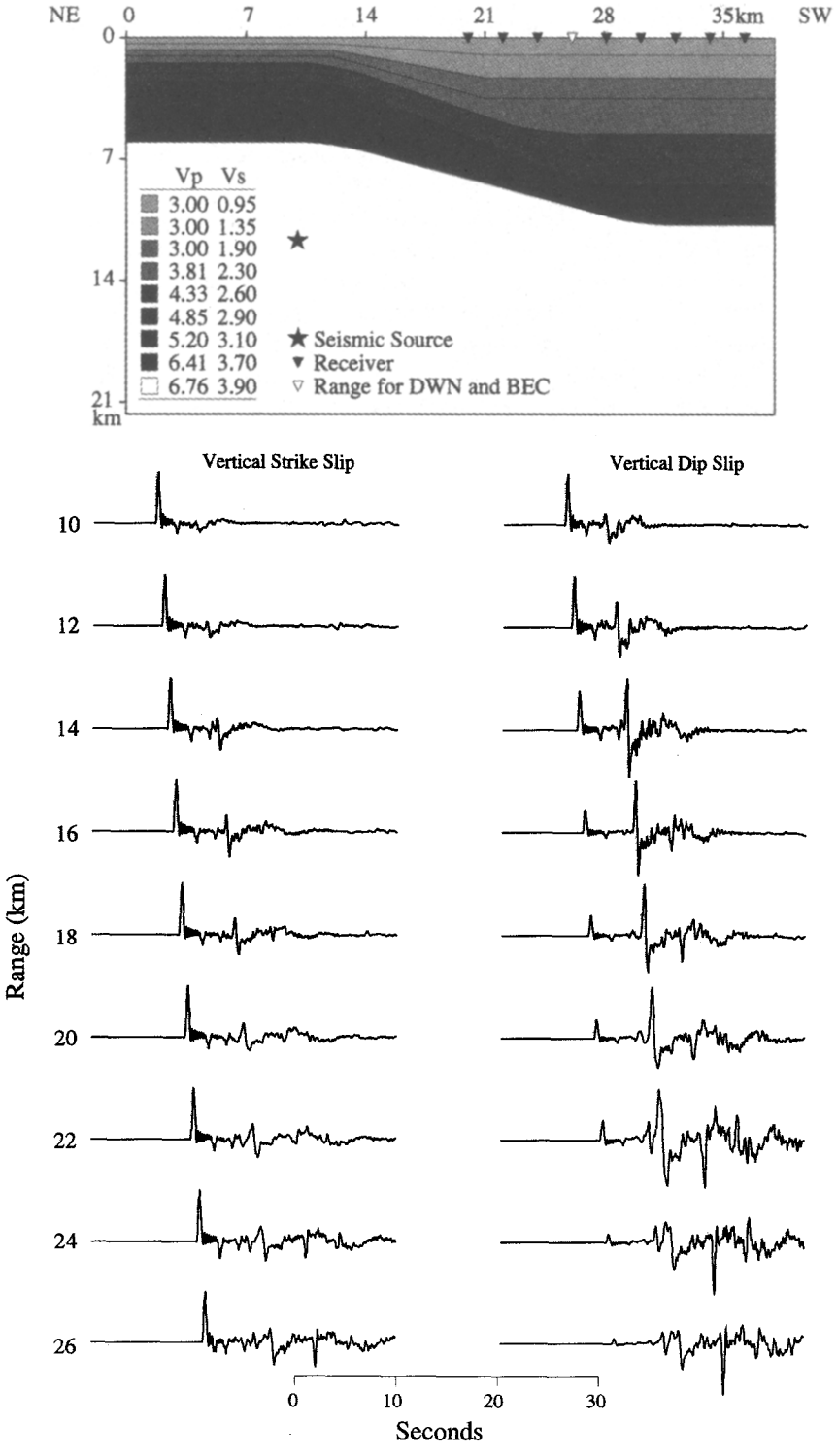

Figure 7. Finite-difference tangential-component synthetic waveforms for two fundamental fault mechanisms produced by the basin edge structure at the top of the figure. NE is to the left. Seismic velocities are given in kilometers per second. Note the large-amplitude multiple in the pure dip-slip synthetics for ranges 14 to 22 km. The slight ringing after the direct S phase is a numerical artifact (grid dispersion) of the finite-difference program.

(a)

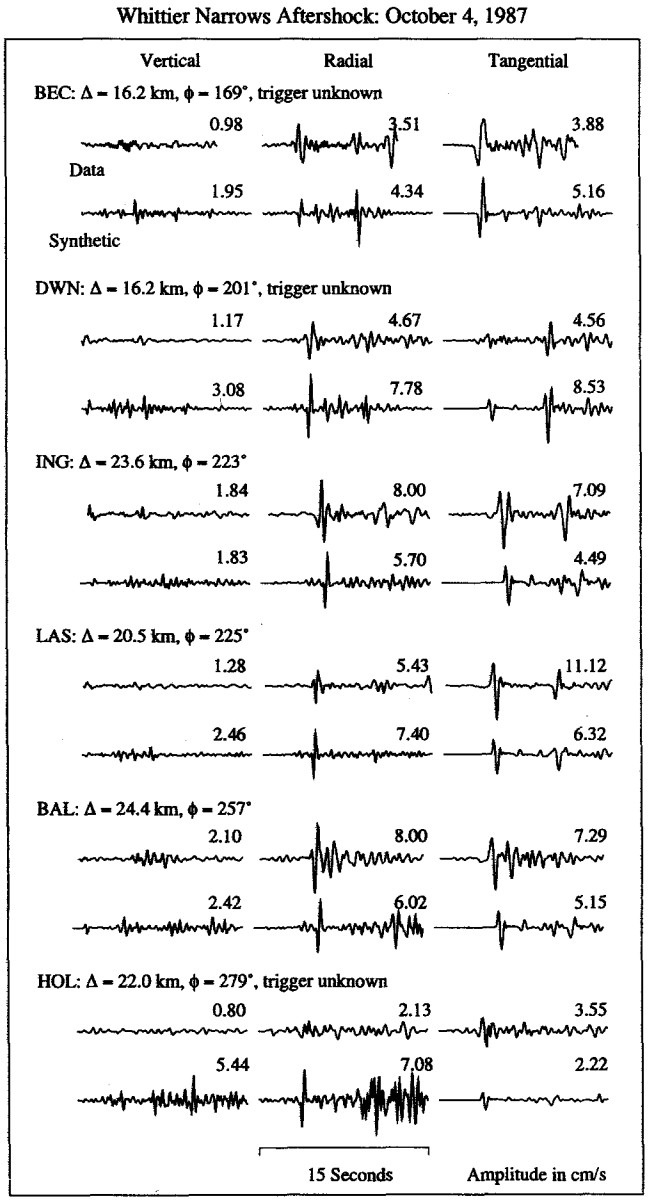

Figure 8. Comparison of velocity synthetic waveforms, produced by the preferred model shown in Figure 7, with 4 October 1987 Whittier Narrows aftershock data. Both data and synthetics have been bandpass-filtered between 0.1 and 3 Hz. A source with $M_0 = 5 \times 10^{23}$ dyn-cm was included in the synthetic waveforms. (a) Comparison for all the stations in the Los Angeles basin used in this study. Both data and synthetic waveforms are plotted at the same amplitude scale. The stations are shown in order of increasing angle of azimuth. The records of ING, LAS, and BAL are shown in absolute time starting 5 sec after the earthquake origin time. The trigger times of BEC, DWN, and HOL are not available; the data and synthetics for these stations are aligned by the direct S on the tangential component. (b) Comparison for station DWN. The amplitude scale for the synthetic waveforms is twice as large as the scale for the data. The dashed lines indicate the timing of direct S.

(b)

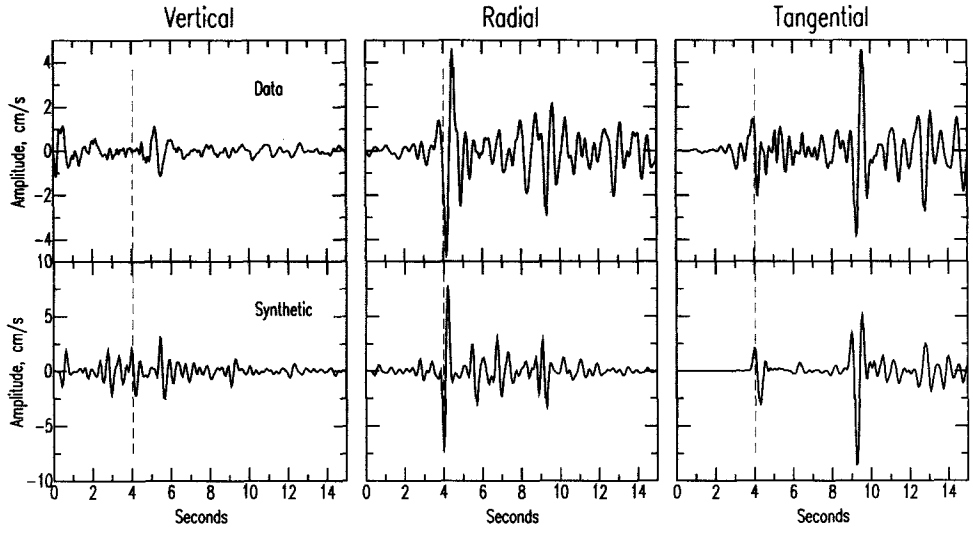

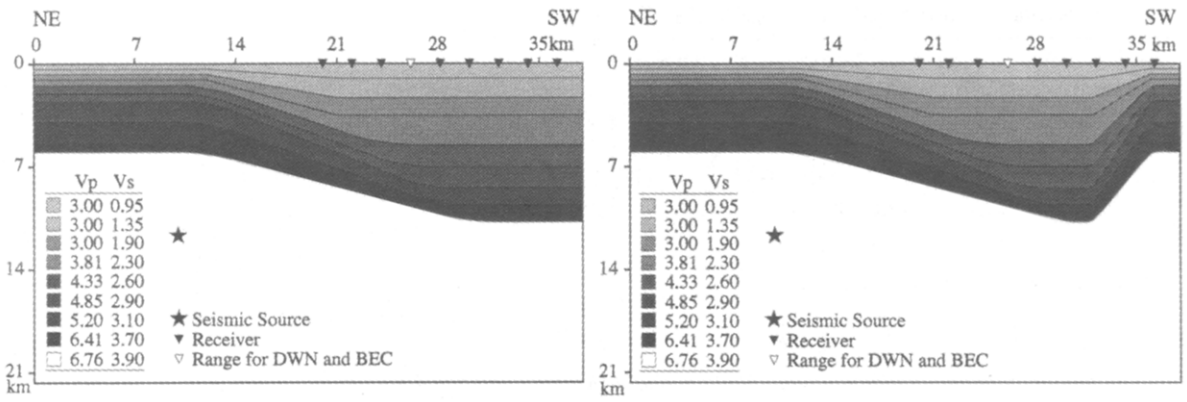

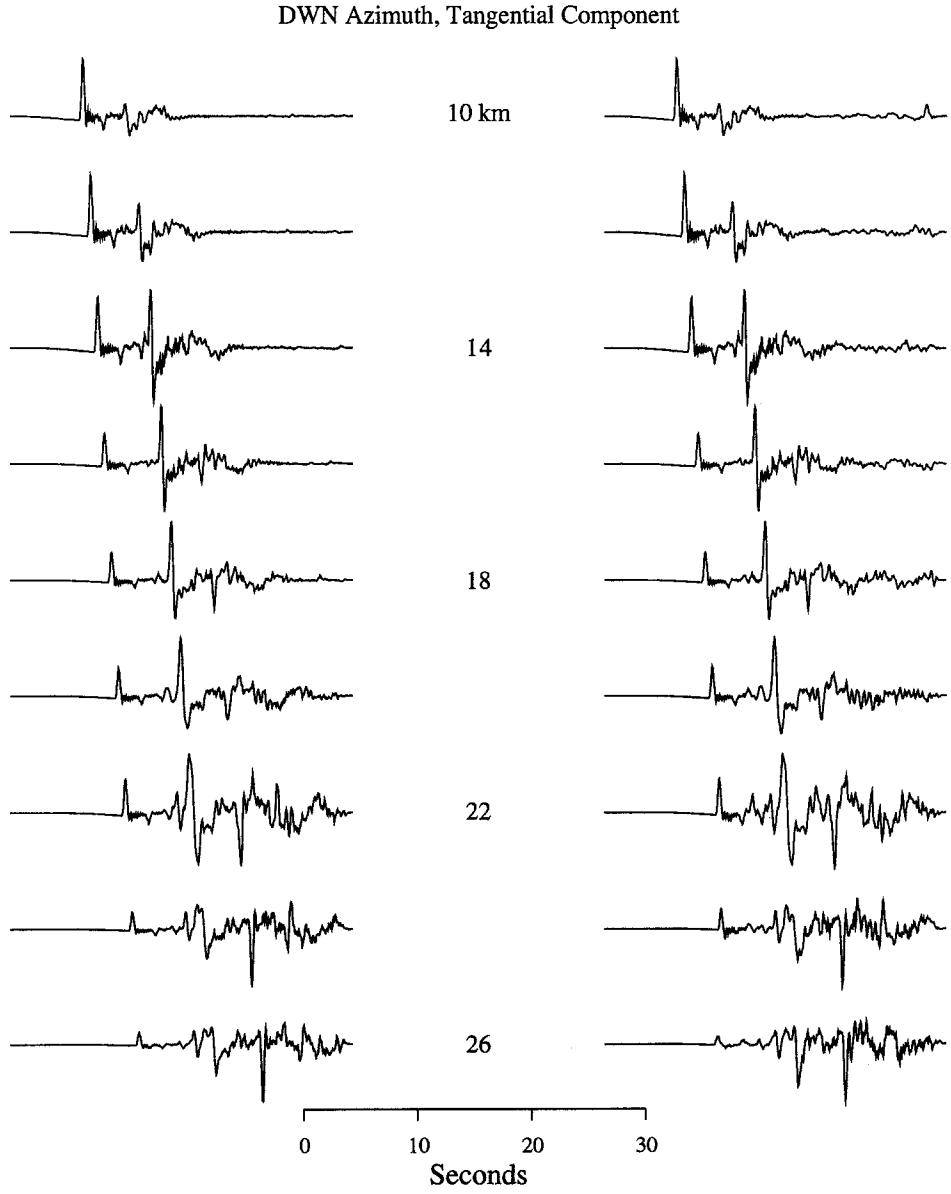

Figure 9. Synthetic waveforms of the tangential component for stations along the DWN azimuth for two models. The model on the left is the one used to produce the synthetics in Figures 7 and 8. In the model on the right, a steep SW edge is included in the basin velocity structure.

the wave train in the Los Angeles basin (see Vidale and Helmberger, 1988), but not change the initial portion of the synthetic with the strong multiple. Overall, for both models, the strong *S* multiple persists with similar amplitude and timing relative to the direct *S* arrival as was generated by the Whittier Narrows model.

The Sierra Madre mainshock was not strong enough be recorded well on many of the CDMG stations in the Los Angeles basin. Records for the stations DWN, BAL, and HOL were digitized from the CDMG report (Huang *et al.*, 1991). The tangential-component acceleration records from these stations are compared with synthetic waveforms in Figure 12. A trigger time for the station HOL is known, so the comparison of data and synthetic can be made in absolute time. This comparison makes it clear that HOL triggered after the direct *P*. This also appears to be true for BAL, for which no trigger time is available. By comparison, the record for DWN is more complete. The USC record is most complete, with a trigger time well before the direct *P* and 15 to 20 sec of coda recorded after the peak amplitudes. A strong multiple phase is clearly present in the records from stations DWN, HOL, and USC, and may be present in the waveform from BAL as well. Neither the amplitude nor the timing is as well matched between data and synthetic for the Sierra Madre mainshock as for the 4 October Whittier Narrows aftershock. The synthetic waveforms have a longer high-amplitude coda than is seen in the data. This may be because the model lacks the ridge between the San Gabriel and Los Angeles basins.

Discussion

Vidale *et al.* (1991) argue that in the Los Angeles basin strong site resonance effects control the polarization of received energy at frequencies greater than 1 or 2 Hz, and that the resonance direction at a given station tends to remain similar from event to event. The effect of the focal mechanism is not entirely drowned out by the site resonance, however. By taking the ratio of peak accelerations of the 1 October mainshock (M_L = 5.9) and the 4 October aftershock for stations over the Los Angeles basin, Vidale (1989) isolated the effect of the radiation pattern. These two studies indicate that at high frequencies the site resonance effects are dominant, but the radiation pattern for an earthquake still has a significant effect on the pattern of peak accelerations.

Strong ground motions are complicated by the competing effects of site response and radiation pattern. Tangential-component synthetic waveforms constructed for

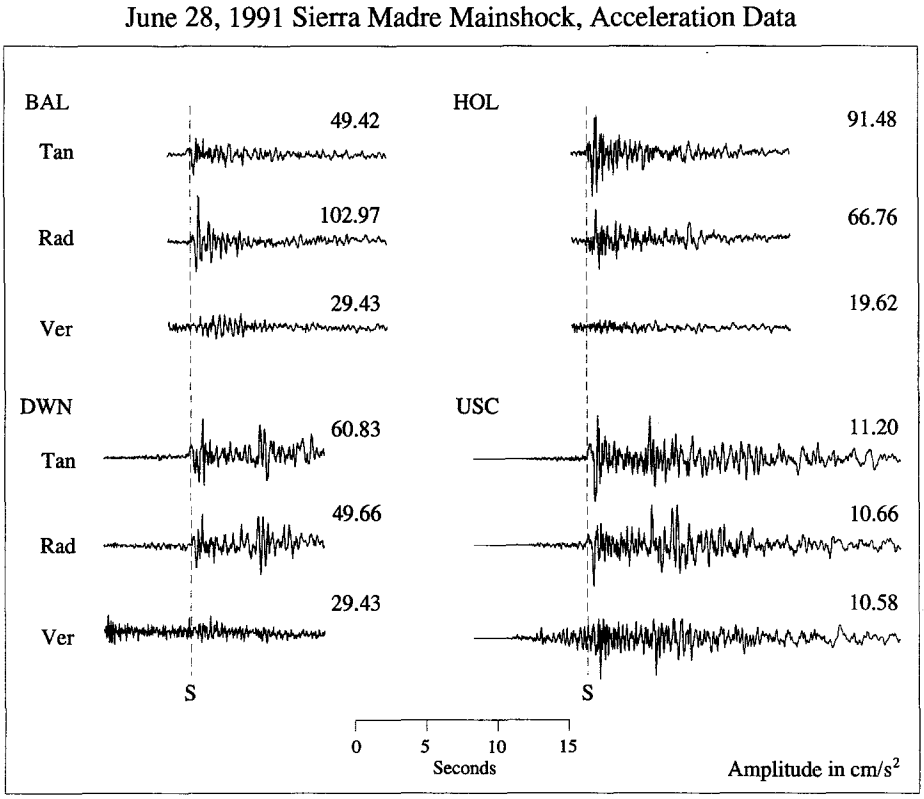

Figure 10. Acceleration data for the 28 June 1991 Sierra Madre mainshock at stations BAL, DWN, HOL, and USC. All records are shown starting from their initial trigger and lined up on the direct *S* arrival. The amplitudes are in centimeters per second squared.

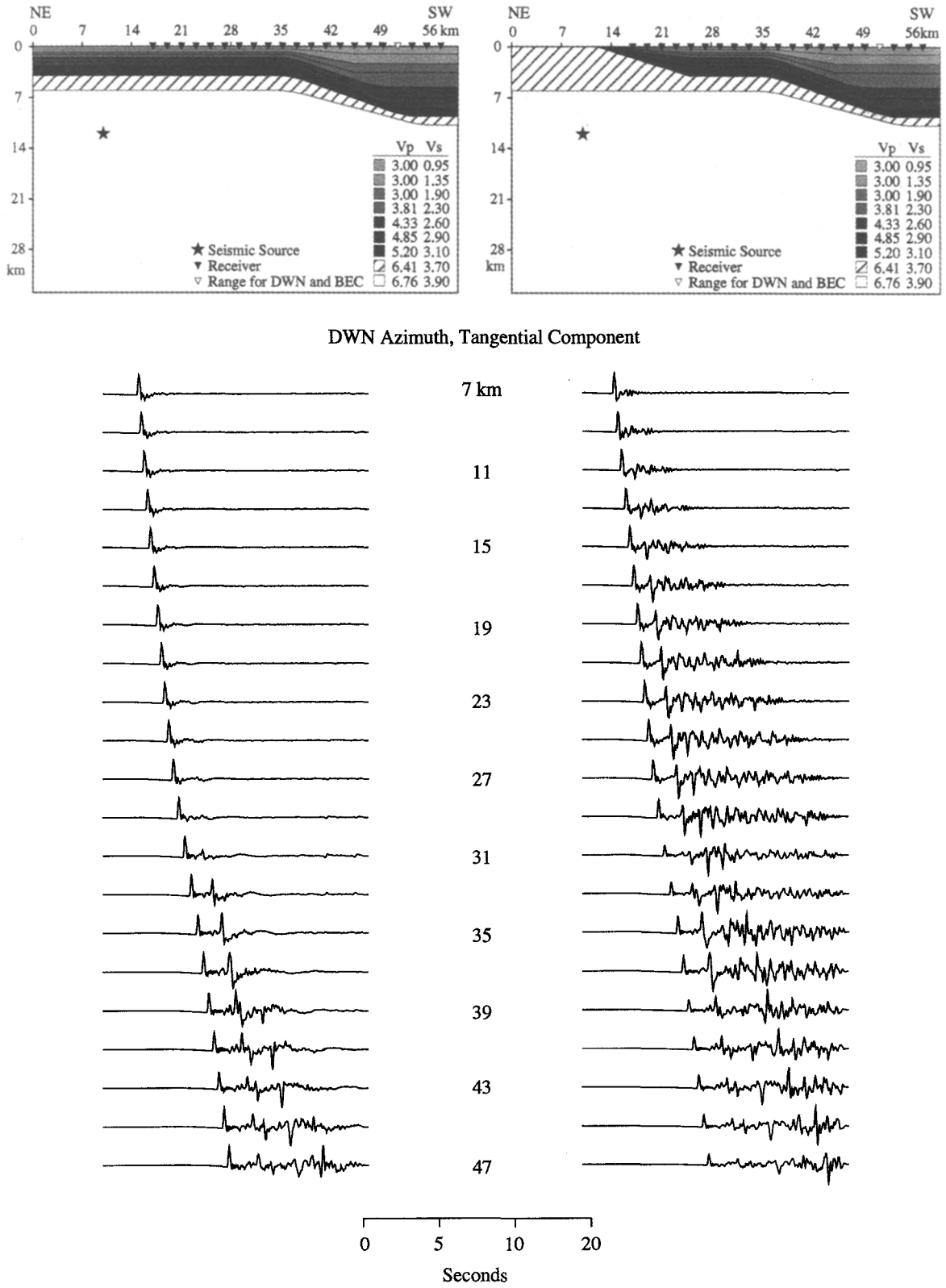

Figure 11. Two models for the velocity structure from the source of the Sierra Madre earthquake into the Los Angeles basin. Seismic velocities given in kilometers per second. The model on the left does not include any structure corresponding to the San Gabriel basin to the NE of the Los Angeles basin. The model on the right includes the northern edge of the San Gabriel basin. The source parameters found by Dreger and Helmberger (1991) are used to calculate the synthetic waveforms. The synthetics are displacement waveforms.

the 1 October Whittier Narrows mainshock with the focal mechanism of the largest subevent (Bent and Helmberger, 1989) predict that there should be no multiple after the direct *S*. Recordings from some stations, however, have a clear multiple. It is possible that the effects of the radiation pattern are being averaged by the three-dimensional basin structure. Figure 13 shows the variation in the amplitude ratio of the *SS* and *S* phases in synthetic waveforms as the focal mechanism is varied. The plots are planes with constant strike, rake, and dip, respectively, slicing through the space of possible source parameters. The plots in the left-hand column intersect in this space at the parameters for the 4 October aftershock, and the plots in the right-hand column intersect at the parameters for the 1 October mainshock. The squares drawn in the figures indicate the intersection point for the planes plotted in that column. These plots predict that the majority of focal mechanisms should generate a multiple (*SS*) with at least half the amplitude of the direct *S*. Only narrow bands in the parameter space correspond to synthetic waveforms with no multiple. In the real world, it appears that waveforms are generated with a radiation pattern that corresponds to an averaged focal mechanism (Liu and Helmberger, 1985). This can be due to variations in the azimuth of the propagation path as slip progresses along the finite fault length, departures of the fault from a simple planar geometry, and multipathing of the energy as it propagates to the receiver. In our case, this means that receivers at a similar epicentral distance and overlying a similar velocity structure should have a visible multiple, regardless of the source mechanism.

The vertical radiation pattern for a vertical strike-slip fault for the *SH* system is a constant dependent on the shear velocity in the source region, but the vertical radiation patterns for the other fundamental fault orientations are all dependent on the ray parameter and apparent slowness (Helmberger, 1983). This effect is evident in Figure 7. For the strike-slip source, the *SS* phase is clearly developed beyond about 14 km and, relative to the direct *S* pulse, its amplitude does not change much. For the dip-slip source, the *SS* phase increases in amplitude relative to the direct arrival over the range from 12 to 18 km. Beyond 18 km, the *SS* phase drops in relative amplitude and a third phase grows to dominate the records. The energy that produces the direct *S* phase is leaving the source in a nearly horizontal direction. This is a node in the dip-slip vertical radiation pattern. By comparison, the multiples are produced by energy propagating upward from the source at angles where the radiation pattern for the dip-slip source is stronger. As the

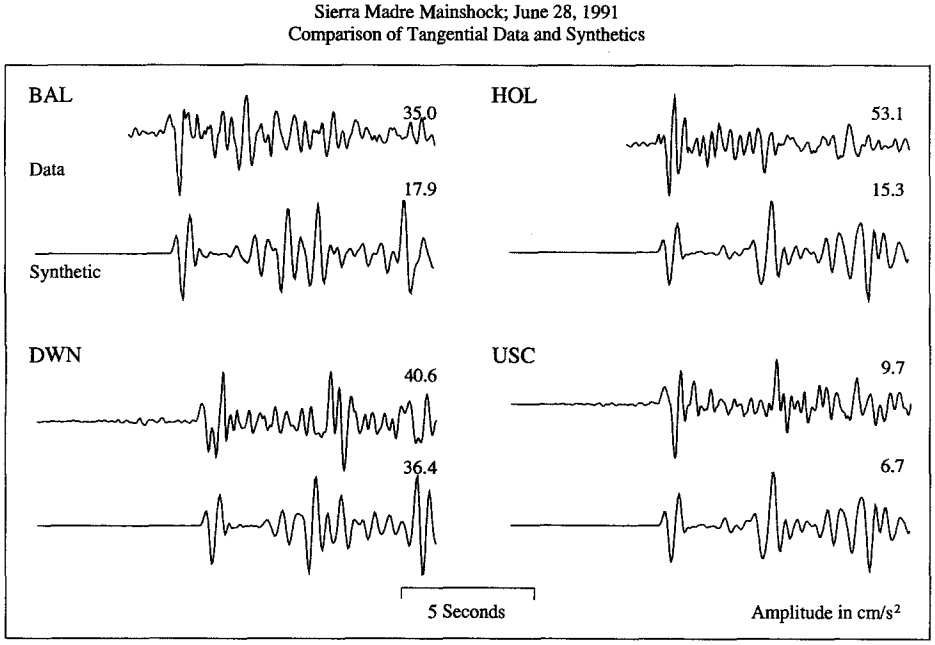

Figure 12. A comparison of acceleration data and synthetic waveforms for the tangential component of the Sierra Madre mainshock. The source parameters found by Dreger and Helmberger (1991) are used to calculate the synthetics. They include a moment of one-third of $M_0 = 2.5 \times 10^{24}$ dyn-cm (see text). Both data and synthetic waveforms have been bandpass-filtered between 0.1 and 3 Hz. No trigger times are available for BAL and DWN. For these stations, the data and synthetics are lined up by the direct *S* arrival. Trigger times are available for HOL and USC. The data and synthetic for HOL are compared in absolute time. However, the USC record is shifted 1 sec to the left in order to line up the direct *S* arrivals of the data and synthetic.

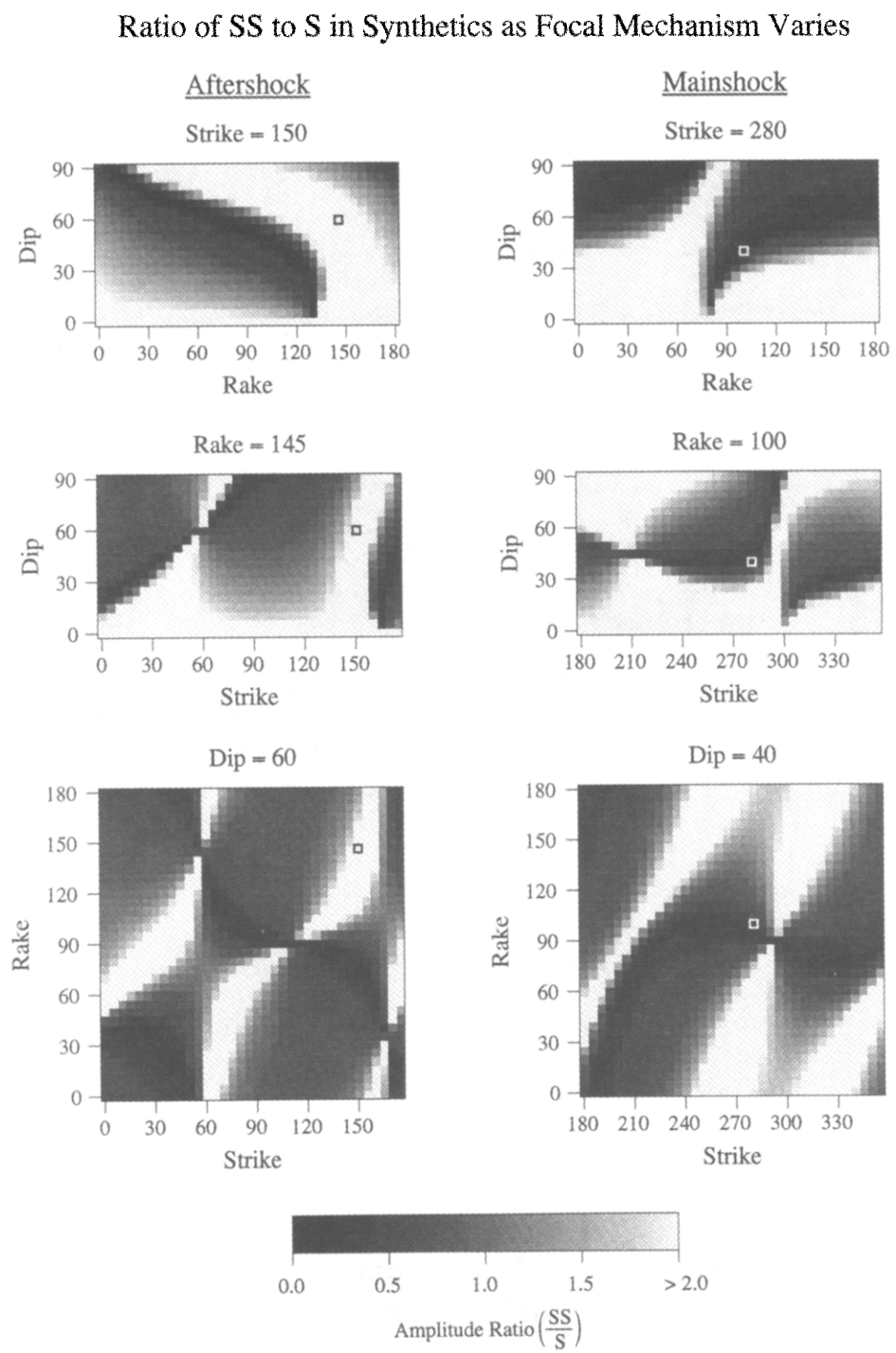

Figure 13. The variation in the amplitude ratio of the *SS* and *S* phases in synthetic waveforms as the focal mechanism is varied. The black areas have little or no multiple, and the white areas have multiples at least twice as large as the direct *S*. The synthetic waveforms were constructed with the velocity model shown in Figure 7 at a range of 16 km (the distance from the Whittier Narrows earthquake sequence to station DWN). The left-hand column of figures show how the *SS*/*S* amplitude ratio changes in the synthetic waveforms if one parameter of the aftershock is held fixed and the other two parameters of the aftershock are allowed to vary. The right-hand column of figures show the variation in the *SS*/*S* ratio when a parameter of the mainshock is held fixed and the other two parameters for the mainshock are varied. The parameters of the largest subevent of the 1 October Whittier Narrows mainshock (Bent and Helmberger, 1989) are used for this purpose. The squares in the figures indicate the locations of the aftershock and mainshock in the parameter space.

range increases, the take-off angle of energy for a particular phase swings toward the horizontal, with correspondingly less radiated energy. A further multiple phase, with a near-vertical take-off angle, may begin to dominate the synthetic.

It is commonly mentioned that an effect of sedimentary basins is to lengthen the waveform coda by setting up surface waves that are trapped to bounce back and forth in the basin. Kawase and Aki (1989), in order to explain observations at Mexico City from the 1985 Michoacan earthquake, examined the response of two types of basins to an incident plane wave and an incident Rayleigh wave. The type 1 basin is a 10-km-long and 1-km-deep trapezoid, with a single velocity throughout, that is embedded in a homogeneous half-space. The type 2 basin is a type 1 basin with a very slow 5-km-long and 250-m-deep trapezoidal layer covering half its surface. They find that a type 1 basin extends the coda noticeably, but not as strongly as a type 2 basin. A type 2 basin is required to explain the extraordinary duration and amplitude of the Mexico City observations. Sanchez-Sesma *et al.* (1988) have very similar findings. Neither a one-dimensional model with a very slow upper layer nor a two-dimensional deep basin (0.5 km) model can explain can explain the Mexico City observation by themselves. Combining a two-dimensional basin with a thin slow velocity cap is much more successful.

In the present study, a comparison is made between a model with one basin edge and a full basin model. There is virtually no difference between the waveforms for these two models, and there is no significant increase in the duration of the coda. Although they do not find that it is effective enough in lengthening the coda to explain the Mexico City observations, Kawase and Aki (1989) do find that the type 1 basin model does significantly extend the coda in comparison to that produced by a one-dimensional model. There are several possible reasons for the difference between the results in this study and that of Kawase and Aki. The full basin model presented here is much deeper than Kawase and Aki's type 1 basin. Our model has a gradational transition of velocity with depth. The largest impedance contrast between layers in the model is only 1.4, while Kawase and Aki use an impedance contrast of 2.5. Also, the velocity layers in our model do not completely pinch out at the basin edges, and energy leaves the basin over this lip. However, it seems unlikely that this aspect of the basin model is very significant because energy also leaks out of the trailing edges of basins (Vidale and Helmberger, 1988). The reason for this can be seen by considering the cartoon in Figure 6, with rays propagating from within the basin toward the basin edge to the left. The same ray geometry that serves to focus energy arriving from outside the basin will defocus rays striking the basin edge from the inside.

Strong motions are often characterized by peak accelerations and coda duration. It is also important, though, to consider the overall envelope and the change in the envelope as the range increases. The type 1 basin of Kawase and Aki (1989) extends the coda in comparison to one-dimensional models, but only with monotonically decaying amplitudes. The very slow, thin layer over half of the basin is required to get a coda with amplitudes as large or larger than the initial portion of the record. Sanchez-Sesma *et al.* (1988) also needed a very slow capping layer to get a coda of extreme length. Their synthetic waveforms vary greatly in amplitude and duration at different receiver positions on the basin model. Our work indicates that very deep basin structures, without a very slow layer at the surface, can generate *S* multiples with amplitudes larger than the direct *S* phase. These synthetic waveforms are not of extremely long duration, but as the range increases further multiples increase in amplitude to dominate the record. As a result, a large event with multiple subevents distributed over a broad fault plane could generate long wave trains in the Los Angeles basin with significant variations in the waveform envelope from point to point in the basin. Another complication of basin structure not addressed here is the role of attenuation, especially shallow attenuation and scattering. Some discussion of this is given by Frankel and Vidale (1992), but our strategy is to establish the basic velocity structure and then add these properties later.

Conclusions

A multiple of the direct *S* phase, seen in data from the Los Angeles basin stations for the 4 October 1987 Whittier Narrows aftershock, can be forward modeled with a two-dimensional velocity structure. An attempt was made to fit absolute *S* and *P* times (when available), *S-P* times, *SS-S* times, the relative amplitude of *S* and *SS*, and the overall absolute amplitude. These parameters in the data are matched well by the synthetic waveforms, though the phase of the *SS* pulse is not. The fit is more erratic for stations in the north part of the basin (further off the cross-section azimuth of about N205°E). The cross section into the basin changes significantly with azimuth from the source of the Whittier Narrows events, and cannot be modeled by a single two-dimensional model.

Basin edge effects are important. Critical angle reflections of energy in the dipping layers at the leading edge of the basin trap energy and turn it sharply back to the receivers. In a section of synthetic waveforms calculated for the 4 October Whittier Narrows aftershock, the amplitude of *SS* is greatest in the deepest part of the basin, where it is two times larger than direct *S*. The coda duration increases from 8 sec to more than 20 sec from the NE to the SW. A full basin model is compared to a model with only a leading basin edge. The full basin model produces no significant increase in coda duration

when compared to the model with a single basin edge. At the far edge of the basin, energy leaks out rather than being strongly reflected back into the basin. The basin edge effect is not significantly different if the earthquake is located away from the basin (e.g., the Sierra Madre mainshock) or immediately adjacent to it (e.g., the Whittier Narrows aftershock).

We have achieved some success in deterministic, forward modeling of these strong-motion records. Such modeling is useful in predicting strong motions of large events in the region and in preliminary efforts in the construction of three-dimensional models. That is, it establishes constraints on the structure of two-dimensional slices cutting through the region to be modeled in three-dimensional analysis. Such model slices could place additional constraints on the three-dimensional model beyond what is available from geologic and borehole data alone.

Acknowledgments

Egill Hauksson provided the data and specifications for the USC record of the Sierra Madre mainshock. The finite-difference code was written by Robert Clayton and John Vidale. Doug Dreger's help with learning to use this code was invaluable. This material is based upon work supported under a National Science Foundation Graduate Research Fellowship. This study was supported by a S.C.E.C. contract through USC Number 569933 funded by NSF EAR 89-20136 and by NSF EAR-9304110. Contribution Number 5380 of the Division of Geological and Planetary Sciences, California Institute of Technology.

References

Anderson, J. G., P. Bodin, J. N. Brune, J. Prince, S. K. Singh, R. Quaas, and M. Onate (1986). Strong ground motion from the Michoacan, Mexico, earthquake, *Science* **233**, 1043–1048.

Bent, A. L. and D. V. Helmberger (1989). Source complexity of the October 1, 1987, Whittier Narrows earthquake, *J. Geophys. Res.* **94**, 9548–9556.

Campillo, M., J. C. Gariel, K. Aki, and F. J. Sanchez-Sesma (1989). Destructive strong ground motion in Mexico City: Source, path, and site effects during great 1985 Michoacan earthquake, *Bull. Seism. Soc. Am.* **79**, 1718–1735.

Davis, T. L., J. Namson, and R. F. Yerkes (1989). A cross section of the Los Angeles area: seismically active fold and thrust belt, the 1987 Whittier Narrows earthquake, and earthquake hazard, *J. Geophys. Res.* **94**, 9644–9664.

Dreger, D. and D. Helmberger (1991). Source parameters of the Sierra Madre earthquake from regional and local body waves, *Geophys. Res. Lett.* **18**, 2015–2018.

Frankel, A. and J. Vidale (1992). A 3-dimensional simulation of seismic-waves in the Santa Clara Valley, California, from a Loma Prieta aftershock, *Bull. Seism. Soc. Am.* **82**, 2045–2074.

Graves, R. W. and R. W. Clayton (1992). Modeling path effects in three-dimensional basin structures, *Bull. Seism. Soc. Am.* **82**, 81–103.

Hauksson, E. (1990). Earthquakes, faulting and stress in the Los Angeles basin, *J. Geophys. Res.* **95**, 15365–15394.

Helmberger, D. V. (1983). Theory and application of synthetic seismograms, in *Earthquakes: Observation, Theory and Interpretation*, Hiroo Kanamori (Editor) Soc. Italiana di Fisica, Bologna, Italy, 173–222.

Helmberger, D., D. Dreger, R. Stead, and H. Kanamori (1993). Impact of broadband seismology on the understanding of strong motions, *Bull. Seism. Soc. Am.* **83**, 830–850.

Helmberger, D. V. and J. E. Vidale (1988). Modeling strong motions produced by earthquakes with two-dimensional numerical codes, *Bull. Seism. Soc. Am.* **78**, 109–121.

Huang, M., A. Shakal, R. Darragh, C. Ventura, T. Cao, R. Sherburne, P. Fung, J. Wampole, M. DeLisle, and C. Petersen (1991). CSMIP strong-motion records from the Sierra Madre, California earthquake of 28 June 1991, *Calif. Div. Mines Geol. Rept. OSMS 91-03*.

Kawase, H. and K. Aki (1989). A study on the response of a soft basin for incident *S*, *P*, and Rayleigh waves with special reference to the long duration observed in Mexico City, *Bull. Seism. Soc. Am.* **79**, 1361–1382.

Liu, H. L. and D. V. Helmberger (1985). The 23:19 aftershock of the 15 October 1979 Imperial Valley earthquake: more evidence for an asperity, *Bull. Seism. Soc. Am.* **75**, 689–708.

Mueller, C., C. Dietel, G. Glassmoyer, T. Noce, E. Sembera, P. Spudich, and J. Watson (1988). Digital recordings of aftershocks of the 1 October 1987 Whittier Narrows, California, earthquake, U. S. Geological Survey, *Dept. Interior Open-File Rept. 88-688*.

Novaro, O., T. H. Seligman, J. M. Alvarez-Tostado, J. L. Mateos, and J. Flores (1990). Two-dimensional model for site-effect studies of microtremors in the San Fernando Valley, Bull. *Seism. Soc. Am.* **80**, 239–251.

Saikia, C. K. (1994). Estimated ground motions in Los Angeles due to $M_w = 7$ earthquake on the Elysian thrust fault, *Bull. Seism. Soc. Am.* **83**, 780–810.

Sanchez-Sesma, F., S. Chavez-Perez, M. Suarez, M. A. Bravo and L. E. Perez-Rocha (1988). The Mexico earthquake of September 19, 1985—on the seismic response of the Valley of Mexico, *Earthquake Spectra* **4**, 569–589.

Shakal, A. F., M. J. Huang, C. E. Ventura, D. L. Parke, T. Q. Cao, R. W. Sherburne, and R. Blazquez (1987). CSMIP strong-motion records from the Whittier, California earthquake of 1 October 1987, *Calif. Div. Mines Geol. Rept. OSMS 87-05*.

Vidale, J., D. V. Helmberger, and R. W. Clayton (1985). Finite-difference seismograms for *SH* waves, *Bull. Seism. Soc. Am.* **75**, 1765–1782.

Vidale, J. E. (1986). Complex polarization analysis of particle motion, *Bull. Seism. Soc. Am.* **76**, 1393–1405.

Vidale, J. E. (1989). Influence of focal mechanism on peak accelerations of strong motions of the Whittier Narrows, California, earthquake and an aftershock, *J. Geophys. Res.* **94**, 9607–9613.

Vidale, J. E., O. Bonamassa, and H. Houston (1991). Directional site resonances observed from the 1 October 1987 Whittier, *Earthquake Spectra* **7**, 107–125.

Vidale, J. E. and D. V. Helmberger (1988). Elastic finite-difference modeling of the 1971 San Fernando, California earthquake, *Bull. Seism. Soc. Am.* **78**, 122–141.

Wald, D. J. (1992). Strong motion and broadband teleseismic analysis of the 1991 Sierra Madre, California, earthquake, *J. Geophys. Res.* **97**, 11033–11046.

Yerkes, R. F., T. H. McCulloh, J. E. Schoellhamer, and J. G. Vedder (1965). Geology of the Los Angeles basin, California—an introduction. *U. S. Geol. Surv. Profess. Pap. 420-A*.

Seismological Laboratory 252-21
Caltech
Pasadena, California 91125

Manuscript received 3 August 1993.